ChemComm

ROYAL SOCIETY OF CHEMISTRY

COMMUNICATION

View Article Online
View Journal | View Issue

Check for updates

Cite this: *Chem. Commun.*, 2024, **60**, 4459

Received 13th February 2024, Accepted 17th March 2024

DOI: 10.1039/d4cc00537f

rsc.li/chemcomm

A novel B,O,N-doped mesogen with narrowband MR-TADF emission†‡

Julius A. Knöller, *[a] Burcu Sönmez,[a] Tomas Matulaitis,[b] Abhishek Kumar Gupta,[b] Eli Zysman-Colman *[b] and Sabine Laschat *[a]

Modification of an unsymmetric B,O,N-doped aromatic core with peripheral mesogenic units triggers self-assembly into a columnar hexagonal mesophase, which is stable between 22 and 144 °C. The columnar assembly is preserved in a glassy state below 22 °C. The B,O,N-doped mesogen displays narrowband sky-blue multiresonance thermally activated delayed fluorescence (MR-TADF) under diluted conditions and bright excimer emission in condensed phase. Our combined experimental and theoretical approach provides insight into the development of strongly aggregating liquid crystalline MR-TADF emitters.

Since their discovery in 1977 by Chandrasekhar *et al.*,[1] discotic liquid crystals (DLCs) have been heavily investigated in the context of functional materials.[2,3] Decoration of a rigid, often aromatic core with flexible side chains results in nanophase segregation where the cores stack into columns that arrange in a 2D lattice *e.g.*, a hexagonal lattice in the case of columnar hexagonal (Col_h) DLCs.[2] The strong electronic overlap of individual mesogens within a columnar stack promotes enhanced charge carrier properties along the columnar axis and thus DLCs have found utility in organic optoelectronic applications.[4–6]

A wide variety of aromatic motifs have been incorporated within DLCs targeted for use as components in organic light-emitting diodes (OLEDs).[6,7] Their distinct self-assembly allows for improved charge transport,[6,7] self-healing[6,7] and enhanced light outcoupling.[8,9] Boron-doped polycyclic aromatic hydrocarbons (B-PAHs),[10–12] have been largely neglected within the development of DLCs save for a triphenylborane derived DLC **1**[13] and a **DOBNA** based DLC **2**[14] (Scheme 1). While **1** demonstrates ambipolar charge-carrier transport, **2** serves as acceptor in donor–acceptor supramolecular polymers.[13,14] Doping PAHs with boron- and electron-donating heteroatoms *e.g.* oxygen in **DOBNA** (Scheme 1) led to the discovery of MR-TADF in 2015[15] and the first MR-TADF OLED in 2016.[16] The antagonistic resonance effects of the heteroatoms induce a small singlet (S_1) and triplet (T_1) energy gap (ΔE_{ST} < 200 meV), allowing for thermally activated delayed fluorescence (TADF) from a short-range charge transfer (SRCT) excited state enabled by reverse intersystem crossing from T_1 to S_1 states. MR-TADF emitters are highly sought after for use in OLEDs due to their ability to harvest both singlet and triplet excitons to produce light[17] and their narrowband emission due to their structural rigidity and their emissive SRCT state.[18,19] While a small number of conventional TADF DLCs and smectic LCs have

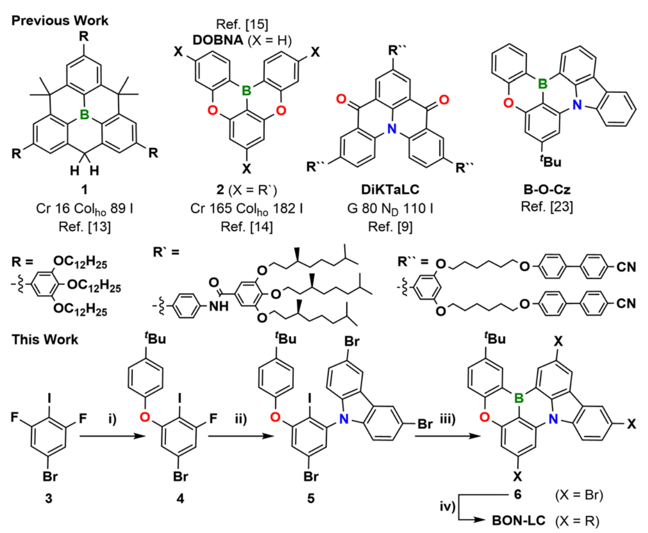

Scheme 1 B-PAH based DLCs **1**, **2**, a boron free MR-TADF LC **DiKTaLC** and MR-TADF emitters **DOBNA** and **B-O-Cz**. Conditions: (i) 4-*tert*-butylphenol, Cs_2CO_3, DMF, 80 °C, 72 h, 49%; (ii) 3,6-dibromo-9*H*-carbazole, Cs_2CO_3, DMF, 80 °C, 72 h (80%); (iii) *n*-butyllithium, BBr_3, *N*,*N*-diisopropylethylamine, 140 °C, 18 h, 48%; (iv) R-BPin, $Pd(PPh_3)_4$ (15 mol%), Cs_2CO_3, toluene: EtOH: H_2O = 2 : 1 : 1, 115 °C, 18 h (42%).

[a] Institut für Organische Chemie, Universität Stuttgart, Pfaffenwaldring 55, D-70569, Stuttgart, Germany. E-mail: sabine.laschat@oc.uni-stuttgart.de
[b] Organic Semiconductor Centre, EaStCHEM School of Chemistry, University of St Andrews, St Andrews, Fife KY16 9ST, UK. E-mail: eli.zysman-colman@st-andrews.ac.uk; Fax: +44-1334 463808; Tel: +44-1334 463826

† Electronic supplementary information (ESI) available. See DOI: https://doi.org/10.1039/d4cc00537f

‡ The research data supporting this publication can be accessed at https://doi.org/10.17630/2d90aafb-a5d2-4645-977d-db424f2020fe.

been reported,[20–22] MR-TADF DLCs based on B-PAHs remain elusive despite their great potential in solution-processed OLEDs – as recently demonstrated with a boron-free, nematic discotic (N_D) MR-TADF DLC **DiKTaLC**[9] improving light out-coupling in a solution-processed OLED (Scheme 1).

To simultaneously shed light on the self-assembly of MR-TADF B-PAHs and the resulting implications for their photophysics, we designed a DLC, **BON-LC**, based on a reported MR-TADF emitter **B-O-Cz** (Scheme 1).[23] The synthesis of **BON-LC** started from fluorobenzene **3**, which was submitted to two S_NAr reactions introducing *tert*-butylphenoxy (intermediate **4**, 49% yield) and dibromocarbazolyl units in compound **5** (80% yield) utilizing Cs_2CO_3 as the base. Next, compound **5** was selectively lithiated with *n*-butyllithium at the more reactive iodinated site and subsequently treated with BBr_3 as well as Hünigs base at 140 °C to yield the brominated BON-core **6**. Finally, three mesogenic units, each bearing three dodecyloxy groups, were grafted onto the aromatic core *via* Suzuki–Miyaura cross-coupling of **6** in the presence of $Pd(PPh_3)_4$, allowing us to isolate **BON-LC** as a yellow wax in 42% yield after column and gel permeation chromatography (analytical GPC purity > 99%).

Investigation of **BON-LC** *via* differential scanning calorimetry (DSC) revealed a glass transition at 22 °C and a clearing temperature of 144 °C during the second heating cycle (Fig. 1a). Complementary analysis of **BON-LC** *via* polarized optical microscopy (POM) during cooling (rate = 10 K min^{-1}) revealed large homeotropic areas with line defects and fan-shaped textures characteristic for columnar mesophases (Fig. 1a) that transformed into platelet textures upon application of a shear force (*cf.* ESI,† Fig. S19d). Wide angle X-ray diffraction (WAXS) measurements confirmed mesomorphic behaviour of **BON-LC** at 25 °C through the presence of a sharp (10) reflection (d = 31.1 Å) in the small angle regime as well as a superposition of a broad halo (d_{halo} = 4.43 Å) and a π–π reflection ($d_{\pi-\pi}$ = 3.49 Å), resulting from the molten alkyl chains and the tightly stacked aromatic cores of **BON-LC**, respectively (Fig. 1b). Small angle X-ray diffraction (SAXS) measurements revealed 6 reflections in addition to the (10) reflection (Fig. 1b), indexed as (11), (20), (21), (22), (31) and (40) reflections of a columnar hexagonal ordered (Col_{ho}) mesophase due to their characteristic $1{:}1/\sqrt{3}{:}1/2{:}1/\sqrt{7}{:}1/\sqrt{12}{:}1/\sqrt{13}{:}1/4$ relationship (Table S4, ESI†).[24] The absent (30) reflection might be explained by superimposed diffraction of different domains within the sample.[25] Consequently, **BON-LC** displays an enantiotropic Col_{ho} mesophase (Fig. 1b) between 22 and 144 °C, with a tight stacking of the aromatic cores ($d_{\pi-\pi}$ = 3.49 Å) and a cell parameter of a = 35.9 Å, much smaller than the molecular diameter (d_{cal} = 52 Å, from the density functional theory, DFT, optimized structure), indicating a high degree of interdigitation of the alkyl domains. Compared to the other two B-PAH based DLCs **1** and **2**, the choice of the unsymmetric core in **BON-LC** did not affect the mode of self-assembly (Col_{ho}). While **1** and **2** both crystallize (T_m = 16 and 165 °C, respectively), the Col_{ho} mesophase of **BON-LC** is preserved in a glassy state, likely due to a complicated packing of the unsymmetric **BON-LC** molecules in the solid state. The different mesophase compared to **DiKTa-LC** (Col_{ho} *vs.* N_D) can be rationalized through the different mesogenic groups: the peripheral cyanobiphenyl units in **DiKTa-LC** trigger nematic behaviour (Fig. 1) whereas the alkoxy chains allow for columnar assembly of **BON-LC**.

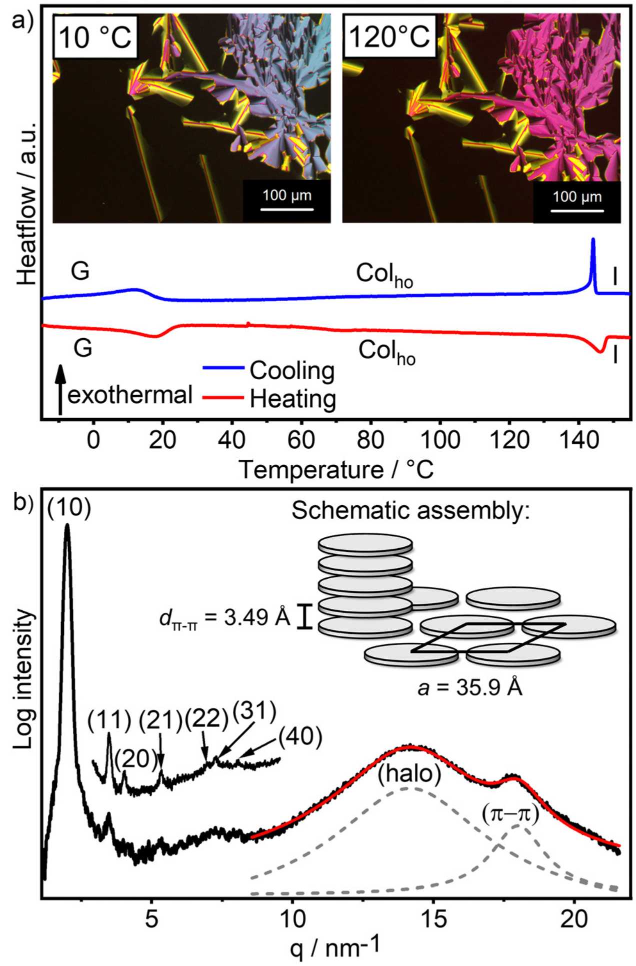

Fig. 1 (a) DSC trace of **BON-LC** (second heating/cooling cycle, rate = 10 K min^{-1}), insets show POM micrographs in the glassy (10 °C) and Col_{ho} (120 °C) phase. (b) WAXS diffractogram of **BON-LC** at 25 °C with magnified SAXS region and fit of the wide-angle regime (red trace) with two Lorentzian functions (dashed grey traces). Inset shows the schematic assembly of **BON-LC** in a Col_{ho} mesophase with the π–π distance d and the unit cell parameter a.

To understand the impact of the aryloxy chains on the photophysics of the MR-TADF core, we modelled the optoelectronic properties of a model system, $\mathbf{BON(OMe)_3}$, at the wPBEPP86 double hybrid (DH) level based on the ground-state optimized structure at the PBE0/6-31G(d,p) level for both $\mathbf{BON(OMe)_3}$ and **BON-LC**. DH calculations for these compounds were found to be faster than the commonly used SCS-CC2 or SCS-ADC2 methods while giving similar results.[26,27] The electron density distribution of the highest occupied and lowest unoccupied molecular orbitals, HOMO and LUMO, of $\mathbf{BON(OMe)_3}$ and **BON-LC** are similarly distributed across the MR-TADF core,[28] while the difference density plots obtained from the DH calculations of $\mathbf{BON(OMe)_3}$ show the characteristic alternating pattern of increasing and decreasing electron density in the excited state compared to the ground state associated with MR-TADF compounds (Fig. S1 and S2, ESI†).[23,29,30] The alkyl chains of the mesogenic units of **BON-LC** are not involved in the HOMO and LUMO distributions (Fig. S2, ESI†). The HOMO and LUMO energies of **BON(OMe)$_3$** are −5.42 and −1.74 eV, respectively, which are somewhat deeper than those of **BON-LC** (−5.21 and −1.67 eV, respectively). The HOMO–LUMO gap, ΔE_g, is thus smaller at 3.54 eV for **BON-LC** compared to **BON(OMe)$_3$** (3.68 eV). The calculated HOMO and LUMO energies of **BON-LC** and **BON(OMe)$_3$** align with the calculated HOMO and LUMO of reported compound **B-O-Cz** (−5.32 and −1.71 eV, at the B3LYP/6-31G level).[23] The calculated energies of the S_1 and T_1 states are 3.28 and 3.33 eV, respectively, resulting in a ΔE_{ST} of **BON(OMe)$_3$** that is close to zero (−0.04 eV) (Fig. S1, ESI†). The high oscillator strength (f = 0.53) for the $S_0 \rightarrow S_1$ transition in **BON(OMe)$_3$** reflects that the S_1 and T_1 states possess SRCT character.

The electrochemical properties of **BON-LC** were investigated *via* cyclic voltammetry (CV) and differential pulse voltammetry (DPV). The CV showed irreversible oxidation and reduction waves, while DPV resolved the first reduction and oxidation processes (Fig. S18 and Table S2, ESI†). From the peak potentials (−1.71/1.13 V *vs.* SCE), the HOMO/LUMO energies were inferred to be −5.93/−1.71 eV for **BON-LC**, values that are slightly destabilized by 0.10/0.14 eV compared to **B-O-Cz** due to the electron-donating nature of the mesogenic groups.[23] Photophysical investigation of the non-aggregated mesogen in dilute toluene solution (c = 0.02 mM) revealed a strong absorption band at λ_{abs} = 448 nm ($\varepsilon = 5.0 \times 10^4$ M cm^{-1}) and a narrow, sky-blue emission band at λ_{PL} = 466 nm typical for the transitions to/from the SRCT excited states of a MR-TADF emitter (Fig. 2).[31] Virtually no solvatochromism during absorption and a weak positive photoluminescence (PL) solvatochromism (Fig. S22c, d and Table S6, ESI†) corroborated the assignment of the excited state as SRCT. The electron-donating mesogenic groups[20] did not induce a long range charge transfer state as occasionally observed for other compounds possessing an MR-TADF core decorated with donor groups.[32,33] The emission band featured a small full width at half maximum (FWHM) of 23 nm (130 meV), a small Stokes shift ($\Delta\bar{\nu}$) of 862 cm^{-1}, and a high PL quantum yield (Φ_{PL}) of 77%. Dispersing **BON-LC** in a polystyrene (PS) matrix (c = 1 wt%) led to a slight bathochromic shift of the absorption and emission maxima (Fig. 2) to λ_{abs} = 454 nm and λ_{PL} = 467 nm, respectively, with an even smaller Stokes shift of $\Delta\bar{\nu}$ = 613 cm^{-1} between the two. Additionally, the emission band was broadened (FWHM = 45 nm or 249 meV), indicating an apparent weak interaction between individual **BON-LC** molecules despite the low doping concentration.[34] The Φ_{PL} increased to 90%, presumably due to the rigid environment of the PS matrix suppressing vibrational relaxation. In stark contrast, the emission band from a neat **BON-LC** film, i.e., where the mesogens tightly stack in a columnar fashion (*vide supra*), was bathochromically shifted to λ_{PL} = 544 nm, broadened (FWHM = 77 nm or 327 meV), and featured a large Stokes shift of $\Delta\bar{\nu}$ = 3596 cm^{-1}. The absorption of the neat film is, in comparison to the absorption in solution and in a PS

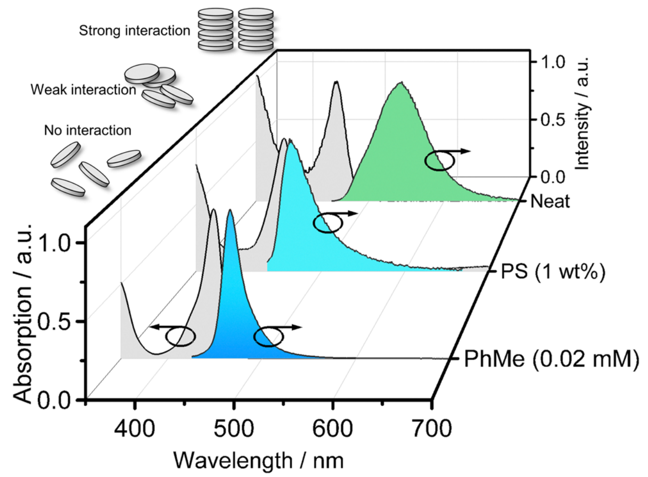

Fig. 2 Absorption (black traces) and emission (blue, cyan and green traces) spectra of **BON-LC** in dilute toluene solution (c = 0.02 mM), in a spin coated polystyrene film (c = 1 wt%) and in a spin coated neat film (λ_{exc} = 350 nm) and a schematic model of the interaction between individual **BON-LC** mesogens (grey disks) in the three investigated systems. The colour of the emission bands corresponds to the observed emission colour.

matrix, virtually unperturbed. The slight bathochromic shift of λ_{abs} = 455 nm indicates only a small degree of interaction in the ground state between the individual molecules despite the tight assembly in the Col$_{ho}$ mesophase. The emission pathway of **BON-LC** in the tightly stacked Col$_{ho}$ glass is thus dominated by excimer formation as often observed for neat MR-TADF materials.[34,35]

We performed PL lifetime experiments *via* time correlated single photon counting (TCSPC, ns regime) and multichannel scaling (MCS, μs regime) measurements to assess whether the observed PL of **BON-LC** was TADF. Only prompt fluorescence was observed for the toluene solution of **BON-LC**, with monoexponential decay kinetics and a prompt fluorescence lifetime (τ_p) of 6.75 ns (Fig. S22b, ESI†). The measured S_1 and T_1 energies of **BON-LC** in glassy toluene at 77 K are 2.58 and 2.51 eV, respectively, resulting in a ΔE_{ST} of 0.07 eV (Fig. S22e, ESI†), smaller than that measured for **B-O-Cz** (ΔE_{ST} = 0.15 eV) in glassy 2-MeTHF.[23] Since many MR-TADF emitters show no TADF in solution, we next investigated the dispersion of **BON-LC** in a PS matrix (c = 1 wt%). The PL decay is complex, modelled as triexponential prompt emission (τ_{avg} = 9.85 ns, Fig. S23b, ESI†), indicating several emissive species *e.g.*, through the hypothesized weak interaction between the individual molecules or different conformations of **BON-LC** locked in the PS matrix. There is a delayed emission (Fig. S23c, ESI†), featuring a monoexponential PL decay with a delayed lifetime (τ_d) of 107.8 μs under vacuum (10^{-5} mbar). The delayed component greatly reduces in intensity in the presence of air, indicating involvement of oxygen-sensitive T_1 states in the photophysical process. Temperature-dependent (77–300 K) time-resolved (Fig. S23d, ESI†) and steady-state PL experiments (Fig. S23e, ESI†) revealed that the delayed component becomes longer with decreasing temperature and the overall emission intensity decreases (although not continuously!), both indicative of an endothermic process that is consistent with TADF.[17] The neat film of **BON-LC** displayed only prompt emission with a double exponential decay and a τ_{avg} = 31.96 ns (Fig. S24b, ESI†), indicating several emissive species in line with the observed excimer formation in the strongly aggregated Col_{ho} glass. Compared to **DiKTa-LC**, the columnar DLC **BON-LC** did not exhibit TADF in the condensed phase. This can be rationalized by the N_D mesophase of **DiKTa-LC** where the peripheral cyanobiphenyl groups effectively shield the MR-TADF cores from each other, thus preserving the photophysical properties of individual **DiKTa-LC** molecules.[9] In stark contrast, the individual **BON-LC** molecules strongly interact in the Col_{ho} mesophase, resulting in excimer emission that did not have a delayed component. Realizing narrowband emission from a MR-TADF core within a naturally strongly aggregating columnar mesogen could therefore prove challenging and require implementing concepts such as a DLC based host-guest system.

In summary, we have designed the first columnar DLC **BON-LC** based on an MR-TADF aromatic core by decoration with mesogenic groups, giving insight into MR-TADF DLCs and B-PAH DLCs simultaneously. The DLC displays an enantiotropic Col_{ho} mesophase between 22 and 144 °C and vitrifies in a glassy state. The specific optoelectronic properties of the MR-TADF core are retained despite the strong electron donating mesogenic groups and **BON-LC** was found to be a bright, sky-blue emitter, displaying MR-TADF in a 1 wt% PS matrix. Self-assembly in the Col_{ho} glass, however, resulted in a loss of the narrowband emission of the monomolecular MR-TADF cores with a broad excimer emission – unfortunately without any delayed emission. We anticipate that this study will inspire future development of MR-TADF DLCs.

Generous financial support by the Studienstiftung des deutschen Volkes, the Ministerium für Wissenschaft, Forschung und Kunst des Landes Baden Württemberg, the Carl Schneider Stiftung Aalen and the DFG (INST 41/897-1, INST 41/1136-1) are gratefully acknowledged. The St Andrews team would also like to thank EPSRC (EP/P010482/1, EP/W015137/1, EP/W007517/1) for financial support. E.Z.-C. was a Royal Society Leverhulme Trust Senior Research Fellow (SRF\R1\201089).

Conflicts of interest

There are no conflicts to declare.

References

1 S. Chandrasekhar, B. K. Sadashiva and K. A. Suresh, *Pramana*, 1977, **9**, 471–480.
2 T. Wöhrle, I. Wurzbach, J. Kirres, A. Kostidou, N. Kapernaum, J. Litterscheidt, J. C. Haenle, P. Staffeld, A. Baro, F. Giesselmann and S. Laschat, *Chem. Rev.*, 2016, **116**, 1139–1241.
3 T. Kato, J. Uchida, T. Ichikawa and T. Sakamoto, *Angew. Chem., Int. Ed.*, 2018, **57**, 4355–4371.
4 W. Pisula, X. Feng and K. Müllen, *Adv. Mater.*, 2010, **22** 3634–3649.
5 R. De and S. K. Pal, *Chem. Commun.*, 2023, **59**, 3050–3066.
6 R. K. Gupta and A. A. Sudhakar, *Langmuir*, 2019, **35**, 2455–2479.
7 R. De, S. Sharma, S. Sengupta and S. Kumar Pal, *Chem. Rec.*, 2022, 22, DOI: 10.1002/tcr.202200056.
8 C. Keum, D. Becker, E. Archer, H. Bock, H. Kitzerow, M. C. Gather and C. Murawski, *Adv. Opt. Mater.*, 2020, **8**, 2000414.
9 D. Chen, F. Tenopala-Carmona, J. A. Knöller, A. Mischok, D. Hall, S. Madayanad Suresh, T. Matulaitis, Y. Olivier, P. Nacke, F. Gießelmann, S. Laschat, M. C. Gather and E. Zysman-Colman, *Angew. Chem., Int. Ed.*, 2023, **62**, e202218911.
10 E. von Grotthuss, A. John, T. Kaese and M. Wagner, *Asian J. Org. Chem.*, 2018, **7**, 37–53.
11 M. Hirai, N. Tanaka, M. Sakai and S. Yamaguchi, *Chem. Rev.*, 2019, **119**, 8291–8331.
12 S. K. Mellerup and S. Wang, *Trends Chem.*, 2019, **1**, 77–89.
13 T. Kushida, A. Shuto, M. Yoshio, T. Kato and S. Yamaguchi, *Angew. Chem., Int. Ed.*, 2015, **54**, 6922–6925.
14 B. Adelizzi, P. Chidchob, N. Tanaka, B. A. G. Lamers, S. C. J. Meskers, S. Ogi, A. R. A. Palmans, S. Yamaguchi and E. W. Meijer, *J. Am. Chem. Soc.*, 2020, **142**, 16681–16689.
15 H. Hirai, K. Nakajima, S. Nakatsuka, K. Shiren, J. Ni, S. Nomura, T. Ikuta and T. Hatakeyama, *Angew. Chem., Int. Ed.*, 2015, **54**, 13581–13585.
16 T. Hatakeyama, K. Shiren, K. Nakajima, S. Nomura, S. Nakatsuka, K. Kinoshita, J. Ni, Y. Ono and T. Ikuta, *Adv. Mater.*, 2016, **28**, 2777–2781.
17 H. Uoyama, K. Goushi, K. Shizu, H. Nomura and C. Adachi, *Nature*, 2012, **492**, 234–238.
18 H. J. Kim and T. Yasuda, *Adv. Opt. Mater.*, 2022, **10**, 2201714.
19 S. Madayanad Suresh, D. Hall, D. Beljonne, Y. Olivier and E. Zysman-Colman, *Adv. Funct. Mater.*, 2020, **30**, 1908677.
20 A. F. Suleymanova, M. Z. Shafikov, A. C. Whitwood, R. Czerwieniec and D. W. Bruce, *J. Mater. Chem. C*, 2021, **9**, 6528–6535.
21 A. F. Suleymanova, M. Z. Shafikov, X. Chen, Y. Wang, R. Czerwieniec and D. W. Bruce, *Phys. Chem. Chem. Phys.*, 2022, **24**, 22115–22121.
22 Y. Zhu, S. Zeng, B. Li, A. J. McEllin, J. Liao, Z. Fang, C. Xiao, D. W. Bruce, W. Zhu and Y. Wang, *ACS Appl. Mater. Interfaces*, 2022, **14**, 15437–15447.
23 J. Park, J. Lim, J. H. Lee, B. Jang, J. H. Han, S. S. Yoon and J. Y. Lee, *ACS Appl. Mater. Interfaces*, 2021, **13**, 45798–45805.
24 N. Godbert, A. Crispini, M. Ghedini, M. Carini, F. Chiaravalloti and A. Ferrise, *J. Appl. Crystallogr.*, 2014, **47**, 668–679.
25 T. Wöhrle, S. J. Beardsworth, C. Schilling, A. Baro, F. Giesselmann and S. Laschat, *Soft Matter*, 2016, **12**, 3730–3736.
26 T. Schwabe and S. Grimme, *Phys. Chem. Chem. Phys.*, 2007, **9**, 3397–3406.
27 M. Kondo, *Chem. Phys. Lett.*, 2022, **804**, 139895.
28 Y. Zhang, D. Zhang, J. Wei, Z. Liu, Y. Lu and L. Duan, *Angew. Chem., Int. Ed.*, 2019, **58**, 16912–16917.
29 K. Shizu and H. Kaji, *Commun. Chem.*, 2022, **5**, 53.
30 S. Oda, B. Kawakami, M. Horiuchi, Y. Yamasaki, R. Kawasumi and T. Hatakeyama, *Adv. Sci.*, 2023, **10**, 2205070.
31 A. Pershin, D. Hall, V. Lemaur, J.-C. Sancho-Garcia, L. Muccioli, E. Zysman-Colman, D. Beljonne and Y. Olivier, *Nat. Commun.*, 2019, **10**, 597.
32 J. A. Knöller, G. Meng, X. Wang, D. Hall, A. Pershin, D. Beljonne, Y. Olivier, S. Laschat, E. Zysman-Colman and S. Wang, *Angew. Chem., Int. Ed.*, 2020, **59**, 3156–3160.
33 S. Wu, W. Li, K. Yoshida, D. Hall, S. Madayanad Suresh, T. Sayner, J. Gong, D. Beljonne, Y. Olivier, I. D. W. Samuel and E. Zysman-Colman, *ACS Appl. Mater. Interfaces*, 2022, **14**, 22341–22352.
34 K. Stavrou, A. Danos, T. Hama, T. Hatakeyama and A. Monkman, *ACS Appl. Mater. Interfaces*, 2021, **13**, 8643–8655.
35 S. Xu, Q. Yang, Y. Zhang, H. Li, Q. Xue, G. Xie, M. Gu, J. Jin, L. Huang and R. Chen, *Chin. Chem. Lett.*, 2021, **32**, 1372–1376.